Acta Geotechnica (2010) 5:1Ð14
DOI 10.1007/s11440-009-0108-1

RESEARCH PAPER

Continuum deformation and stability analyses of a steep hillside slope under rainfall infiltration

Ronaldo I. Borja · Joshua A. White

Received: 20 June 2009 / Accepted: 30 November 2009 / Published online: 8 January 2010

Abstract Rainfall weakens an earth slope in a number of ways. It increases the degree of saturation of the soil, thereby breaking the bonds created by surface tension between the soil particles. When the volume of inÞltrating water is large enough to mobilize ßuid ßow inside the soil matrix, the ßuid exerts a downhill frictional drag on the slope, creating a destabilizing effect. When excess ßuid can no longer inÞltrate the slope due to increased saturation in the soil, it is discharged as a surface runoff and erodes the slope. In this paper, we present a physics-based framework for continuum modeling of a hydrologically driven slope failure similar to what occurred in a steep experimental catchment CB1 near Coos Bay, Oregon. We quantify the rainfall-induced slope deformation and assess the failure potential of the slope using Þnite element modeling that couples solid deformation with ßuid pressure in an unsaturated soil. Results of the studies suggest that for a steep hillside slope underlain by a shallow bedrock similar to the CB1 site, failure would occur by multiple slide blocks with the failure surfaces emerging on the slope face. These results suggest that an inÞnite slope mechanism would be insufÞcient to represent the failure kinematics for a slope similar to CB1.

Keywords Coupled formulation · Rainfall inÞltration · Slope stability · Stabilized Þnite elements · Unsaturated soil

R. I. Borja (✉) · J. A. White
Department of Civil and Environmental Engineering, Stanford University, Stanford, CA 94305, USA
e-mail: borja@stanford.edu

1 Introduction

Hydrologically driven slope instability threatens lives and property worldwide. Examples of large-scale slope failure all over the world are numerous. Landslides in the San Francisco Bay Area during the January 1982 storm resulted in 24 fatalities and millions of dollars in property damage [18, 61]. In January 4, 1982, a 0.22-m storm superimposed on approximately 0.6 m of pre-storm seasonal rainfall triggered thousands of landslides in the central Coast Ranges of California. In Mameyes, Puerto Rico, 1985, rainfall intensity as high as 0.56 m within a 24-h period, with rates as high as 70 mm/h, triggered debris ßows and resulted in 129 deaths [31]. In Rio Limon, Venezuela, 1987, rainfall as much as 0.174 m in less than 5 h triggered numerous shallow landslides and debris ßows resulting in 210 deaths [58]. In Antofagasta, Chile, 1991, rainfall rates as great as 60 mm/h during a 3-h period triggered landslides that resulted in 101 deaths [36]. In Vargas, Venezuela, 1999, a heavy rainfall exceeding 0.9 m over a 3-day period, with daily values greater than the 1,000-year return period [41], triggered thousands of landslides and resulted in an estimated 30,000 deaths [35]. And in 2006, a heavy rainfall in Guinsaugon, Philippines, triggered massive landslides burying an elementary school that had 246 students and 7 teachers [37].

Despite decades of extensive slope-stability model development, the fundamental controls connecting the hydrologic and geotechnical processes triggering slope failure are still not well quantiÞed. This is evident from the La Conchita landslide of January 11, 2005, in southern California that occurred without warning. This lack of understanding is a direct result of the simpliÞed physics in current models, with the omission of the effect of partial saturation from slope-stability calculations. It is known that

increasing the degree of saturation decreases the capillary pressure, which in turn weakens the slope. Moreover, ßuid ßow generates frictional drag on the soil matrix, thus increasing the load that the soil is expected to carry. Despite the expected signiÞcant impact, such interplay between the increase in saturation accompanied by ßuid ßow and increase in potential for slope failure is yet to be fully quantiÞed.

Rainfall-triggered slope instability has been the subject of intense research for many years. Several studies are available concerning Þeld observations and laboratory experiments (e.g., [4–7]). The modeling of the slope failure process has been addressed in a variety of ways over the years. The most common approach is to uncouple the ßuid ßow and slope-stability problems, and instead treat them in a sequential fashion. First, a representative pore-pressure Þeld is determined using either Þeld-observations, analytical solutions, or numerical methods. The Þxed pore-pressure Þeld is then used to determine slope stability either analytically or numerically. Among these uncoupled methods, the most common treatment of the slope-stability sub-problem is through a limit equilibrium approach. For example, see [29, 59] where inÞnite slope approximations are used, and [17] where a simpliÞed Janbu method of slices is used. In [35, 49], a Þnite element solution for the transient sub-surface seepage is combined with a method of slices to determine a slopeÕs factor of safety. The key advantage of these methods is their simplicity. Because the solid and ßuid sub-problems are uncoupled, sophisticated methods and software that have been developed over the years for the separate problems can be brought together. These models also have relatively few parameters to calibrate, and solutions can be computed inexpensively. Furthermore, it is easy to compute parameter sensitivities and understand basic trends in the slope failure process. On the downside, these models make many simplifying assumptions about the slope geometry, the coupled nature of the failure process, the constitutive behavior of the soil, and the in situ stress conditions.

In this paper, we develop and test a 3D physics-based slope deformation model that couples solid deformation with ßuid ßow in variably soils. We also assess the potential of the coupled model to realistically quantify stresses and deformation necessary to trigger slope failure. We emphasize the continuum nature of the modeling approach in that it does not quantify the factor of safety of the slope per se, unlike methods based on limit equilibrium concepts. Instead, our model predicts the spatial and temporal variations of internal stresses, pore water pressure, degree of saturation, and deformation within the slope, as functions of the spatially and temporally varying rainfall intensity. Thus, instead of having one scalar quantity called factor of safety, we assess the failure potential of a given slope based on the stresses and deformation arising from a prescribed forcing function (i.e., rainfall intensity). Stability criteria based on deformation bands are used in this paper to assess the potential for slope failure.

To assess whether the proposed model can successfully integrate important variables in a physics-based characterization of the Þeld conditions and still obtain a realistic description of slope failure, we test the approach with comprehensive and exhaustive data from the Coos Bay experimental catchment (CB1) [21, 22]. The highly instrumented site was originally chosen as a hillslope-scale ÔÔlaboratoryÕÕ for conducting sprinkling experiments aimed at developing and testing hydrologic response models. Experimental and Þeld data generated from the site are plentiful, albeit most of them pertain to hydrologic response data [3, 43, 64]. However, the highly instrumented CB1 slope failed as a large debris ßow in November 1996, raising some interesting questions related to the geotechnical aspects of the site. Given what we know about the topography, hydrologic constraints, and the geotechnical outcome at CB1, this case study seems ideal to test the proposed continuum slope model. However, it must be noted that despite much effort to constrain the site with extensive Þeld instrumentation and investigation, much uncertainty remains particularly with respect to the geotechnical and hydrologic boundary conditions appropriate for the site. Therefore, to underscore what we still do not know about CB1, we emphasize that the analysis reported in this paper pertains only to a slope similar to CB1, and not to the slope at CB1 itself.

The slope at CB1 is steep, on the order of 43 degrees. Any critical state soil mechanics model would predict an initial stress condition within the slope that lies on the ÔÔdilatant sideÕÕ of the critical state line because of the high shear stress to effective-mean-normal stress ratio generated by the steep slope condition [32, 44]. It would thus be reasonable to characterize the constitutive response of the soil skeleton with a MohrÐCoulomb plasticity or similar models, since the compression cap is unlikely to be activated particularly when the effective-mean-normal stress decreases further as a result of the loss of suction with increased saturation. A simpler plasticity model such as the MohrÐCoulomb model also requires fewer material parameters than any of the more sophisticated constitutive models available in the literature (see [76]). For the soil at CB1, which is mostly colluvium, laboratory-determined values of friction angle are available [53, 54]. Furthermore, representative values of lateral root cohesion in clearcut forests in the Oregon Coast Range have been estimated in [55]. Finally, the thickness of the colluvium at CB1 is known to be much smaller than the plan area of the mobilized slide, thus making a continuum analysis approach appropriate for this problem.

2 Continuum slope model

For a solid–water–air mixture the constitutive stress tensor $\boldsymbol{\sigma}'$ (positive for tension) may be defined as

$$\boldsymbol{\sigma}' = \boldsymbol{\sigma} + \left(1 - \frac{K}{K_s}\right)\overline{p}\mathbf{1}, \quad \overline{p} = \psi^w p_w + (1-\psi^w)p_a, \qquad (1)$$

where $\boldsymbol{\sigma}$ is the total Cauchy stress tensor, ψ^w is the degree of saturation, K and K_s are the elastic bulk moduli for the solid matrix and solid constituent, respectively, p_w and p_a are the intrinsic pore water and pore air pressures, respectively, and $\mathbf{1}$ is the Kronecker delta tensor. Borja [11, 15] demonstrated this expression for the constitutive stress tensor to be energy-conjugate to the solid rate of deformation. Under special cases $\boldsymbol{\sigma}'$ reduces to Bishop's stress when $K/K_s = 0$ (incompressible solid grains) and $\psi^w = \chi$; to the Skempton [60] and Nur-Byerlee [45] stress when $\psi^w = 1$; and to the Terzaghi [62] stress when $K/K_s = 0$ and $\psi^w = 1$. The Bishop parameter χ can be determined experimentally [6, 40], and the substitution of degree of saturation ψ^w in lieu of this parameter is a simplified approximation derived from the volume averaging over a so-called representative elementary volume, REV. For purposes of constitutive modeling of the soil layer, we will use the Bishop stress ($K/K_s = 0$), with $\chi = \psi^w$.

Ignoring inertia forces and setting p_a equal to the atmospheric pressure (i.e., zero) for near-surface conditions, balance of linear momentum in the sub-surface is given by the equation

$$\nabla \cdot \boldsymbol{\sigma} + \overline{\rho}\mathbf{g} = 0, \qquad \overline{\rho} = \phi^s \rho_s + \phi^w \rho_w, \qquad (2)$$

where ϕ^s and ϕ^w are the solid and water volume fractions in the REV, respectively, ρ_s and ρ_w are the intrinsic solid and water mass densities (i.e., mass of constituent per unit volume of constituent), respectively, $\overline{\rho}$ is the total mass density of the mixture (ignoring the mass of air phase); and $\mathbf{g}$ is the gravity acceleration vector. Assuming that water is incompressible, balance of water mass in the sub-surface takes the form [10, 11]

$$\frac{\mathrm{d}\phi^w}{\mathrm{d}t} + \phi^w \nabla \cdot \boldsymbol{v} + \nabla \cdot \boldsymbol{q}^w = \pm\theta^b \pm \theta^e, \qquad (3)$$

where $\boldsymbol{v}$ is the velocity of the solid matrix, $\boldsymbol{q}^w = \phi^w(\boldsymbol{v}^w - \boldsymbol{v})$ is the relative discharge velocity, θ^b is the specified rate source/sink, θ^e is the rate of water exchange with the surface continuum, and $\mathrm{d}(\cdot)/\mathrm{d}t$ denotes a material time derivative following the solid motion. The relative discharge velocity is given by the constitutive equation

$$\boldsymbol{q}^w = k_{rw}\boldsymbol{K} \cdot \nabla\left(\frac{p_w}{\rho_w \mathrm{g}} + z\right), \qquad (4)$$

where $\boldsymbol{K}$ is the hydraulic conductivity of the porous medium at complete saturation, k_{rw} is the relative permeability that varies with degree of saturation ψ^w, g is the gravity acceleration constant, and z is the vertical coordinate. The two independent variables of the formulation are the solid velocity $\boldsymbol{v}$ and pore water pressure p_w, satisfying the two balance laws (2) and (3), along with the appropriate boundary and initial conditions. The solution is fully coupled in the sense that the independent variables are determined simultaneously. However, the governing equations must be closed by introducing a pair of constitutive laws determined from continuum principles of thermodynamics [10, 11, 15, 26, 27, 30, 34, 39, 46]: (a) a constitutive law relating the Cauchy effective stress rate tensor $\overset{\circ}{\boldsymbol{\sigma}}{}'$ with the strain rate tensor $\nabla^{\mathrm{s}}\boldsymbol{v}$ for the solid matrix; and (b) a constitutive law relating the suction stress $s = p_a - p_w$ with degree of saturation ψ^w. The second constitutive law is determined from the imbibition portion of the soil-water retention curve for a given soil [7, 67].

Continuum principles of thermodynamics suggest an elasto-plastic constitutive framework for the soil skeleton given by a yield function of the form [10, 11, 15, 26, 27]

$$F(\boldsymbol{\sigma}', s, \overline{p}_c) = 0, \qquad (5)$$

where $\overline{p}_c$ is a stress-like plastic internal variable that determines the size of the compression cap. The suction stress has a positive value for negative pore water pressure (e.g., above the water table) and approaches zero as the soil approaches perfect saturation. However, as noted earlier, the compression cap is not likely to be activated for steep hillside slope conditions, and thus, this explicit dependence of the yield surface on the suction stress may be ignored when using the Mohr–Coulomb or similar yield criteria. We emphasize, however, that the yield function still depends on the suction stress through the Cauchy effective stress tensor $\boldsymbol{\sigma}'$.

Mixed finite element (FE) equations may be readily developed from the variational forms of (2) and (3). The independent variables in the present case are the nodal solid displacement vector $\boldsymbol{d}$ and nodal pore water pressure vector $\boldsymbol{p}$. The coupled FE equations take the form

$$\boldsymbol{F}_{\mathrm{INT}}(\boldsymbol{d}) + \boldsymbol{G}\boldsymbol{p} = \boldsymbol{F}_{\mathrm{EXT}}, \qquad (6)$$

$$\boldsymbol{G}^{\mathrm{T}}\dot{\boldsymbol{d}} + \boldsymbol{M}\dot{\boldsymbol{p}} + \Phi\boldsymbol{p} = \boldsymbol{G}_{\mathrm{EXT}}, \qquad (7)$$

where $\boldsymbol{F}_{\mathrm{INT}}(\boldsymbol{d})$ is the internal nodal force vector arising from the effective stress $\boldsymbol{\sigma}'$, $\boldsymbol{G}$ and $\boldsymbol{G}^{\mathrm{T}}$ are the discrete gradient and discrete divergence operators, respectively, which depend on $\boldsymbol{p}$ through the degree of saturation ψ^w in the unsaturated regime, $\boldsymbol{M}$ is a coupling matrix that vanishes at full saturation, Φ is an effective conductivity matrix that also depends on the degree of saturation, and $\boldsymbol{F}_{\mathrm{EXT}}$ and $\boldsymbol{G}_{\mathrm{EXT}}$ are prescribed vectors of momentum and fluid supplies. Note that the degree of coupling implied by the earlier equations is more intricate than in the fully

saturated case because of the presence of ϕ^w in many terms.

The coupled formulation presented earlier requires mixed finite elements with nodal pressure and displacement degrees of freedom. Low-order mixed finite elements with equal order interpolation for displacement and pressure, would be ideal particularly in 3D when the number of equations can increase dramatically. Unfortunately, low-order mixed finite elements create a numerical difficulty in that in the limit of full saturation and either low permeability or fast loading rates, the pore fluid can impose near or exact incompressibility on the deformation of the solid matrix and create spurious pore-pressure oscillation. To address this difficulty, we use a stabilization scheme proposed by White and Borja [73] based on the concept of polynomial pressure projections (PPP), which was originally proposed in [8, 9, 20] to stabilize the Stokes problem. The primary motivation for using stabilization is computational efficiency: with this technique, it would now be possible to use low-order finite elements, such as those shown in Fig. 1, without the undesirable pore-pressure oscillation that otherwise afflicts the solution without stabilization.

3 Hydrologic and geotechnical conditions at CB1

The CB1 experimental catchment [3, 43, 64], clearcut in 1987, is located along Mettman Ridge approximately 15 km north of Coos Bay in the Oregon Coast Range (Fig. 2). CB1 is a 51-m long (860 m^2) unchanneled valley, with a north-facing aspect, that has an average slope of 43° (see Fig. 3). Three sprinkling experiments were conducted at CB1: experiment #1 conducted in May 1990 at 1.5 mm/h for 6 days; experiment #2 conducted in May 1990 at 3.0 mm/h for 4 days; and experiment #3 conducted in May 1992 at 1.7 mm/h for 7 days. The instrumentation at CB1 used to characterize the spatial and temporal variability in near-surface hydrologic response for the three experiments included an exhaustive grid of rain gauges, piezometers, tensiometers, TDR wave guide pairs (for estimating soil-water content), lysimeters, meteorological sensors (on a tower), atmometers, and weirs. Continuous measurements

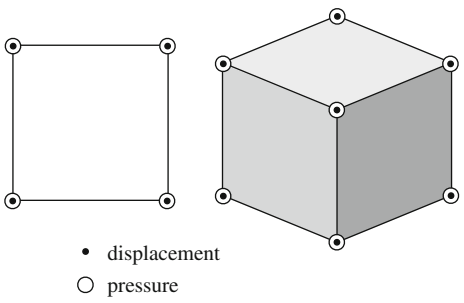

Fig. 1 Stabilized low-order mixed finite elements for coupled solid-deformation/fluid-diffusion: four-node quadrilateral for 2D (*left*), and eight-node hexahedral for 3D (*right*). After White and Borja [73]

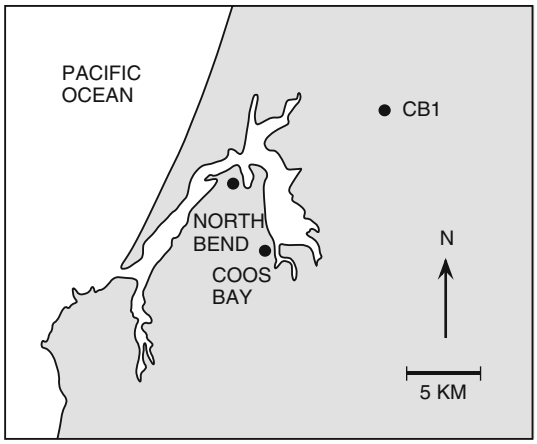

Fig. 2 Location map for CB1 experimental catchment near Coos Bay in the Oregon Coast Range, USA. Reproduced from Ebel et al. [21]

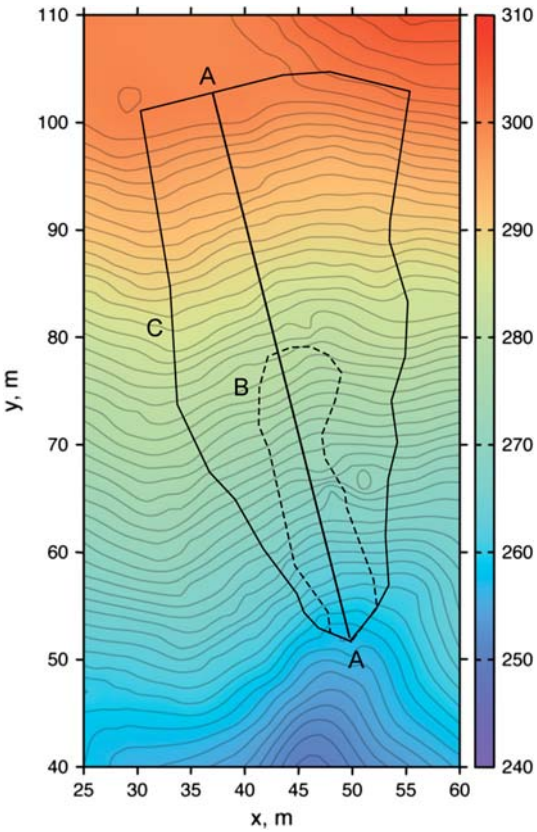

Fig. 3 Topographic map for CB1 experimental catchment. Two-dimensional plane strain condition is assumed along section A-A for the coupled solid deformation-fluid flow analysis. *Dashed curve* B delineates the extent of debris flow zone at CB1 from event of November 1996. Larger region C defines the boundary of the Ebel et al. [22] 3D hydrologic FE model. *Color bar* is elevation in meters

from rainfall, discharge, and total head (from selected piezometers) are available from 1990 through 1996. In November 1996, the CB1 slope failed as a large debris ßow. The instrumentation at CB1 provides one of the most comprehensive hydrologic response data sets in existence for a steep, deforested catchment that has experienced slope failure.

The sediment at CB1 is colluvium, a surÞcial sediment derived from weathered or fresh bedrock, and the soil has no input from aeolian transport. The parent rock for the colluvium is an Eocene turbidite sandstone from the Tyee and Flournoy formations [55]. The soils are well mixed, non-plastic (plasticity index of 0), and gravelly sands [54]. The geometry and thickness of the colluvium are well deÞned from soil borings. Saturated hydraulic conductivity were determined from slug tests, soil-water content, and porosity from TDR measurements, and hysteretic capillary pressure relationships were established from experiments. Discharge chemistry data suggest that runoff generation occurs primarily from water stored in small, poorly connected pores, and fractures in the bedrock, and saprolite connecting with larger macropores during storms [42]. Tracer data (bromide and isotopically tagged water) suggest that the two most important ßow paths at CB1 are rapid saturated ßow through the shallow, fractured bedrock, and vertical percolation in the vadose zone [2]. Piezometer records show that sub-surface storm ßow in the shallow, fractured-rock zone exerts the most signiÞcant control on pore-pressure development in the CB1 colluvium [42]. Tensiometer data indicate that the ßux of water through the unsaturated zone provides an additional control on pore-pressure development and cannot be ignored in slope-stability assessment models [63].

Low conÞning stress triaxial shear tests demonstrate that the colluvium at CB1 is cohesionless (consisting of a sandy matrix with a friction angle of 38° [53, 54]. Lateral root cohesion in clearcut forests in the Oregon Coast Range was estimated to be uniformly less than 10 kPa [55] and may have explained how such a steep slope at CB1 could be sustained by the sediment (apart from the capillary tension that develops in the vadose zone). Low conÞning stress triaxial tests gave an internal friction angle of 40° and zero cohesion [55]. This is in agreement with other measurements near the site that gave internal friction angles ranging from 35Ð44° [19, 57, 74, 75] and zero cohesion [75]. The stress-strain behavior, observed in low conÞning stress triaxial strength testing, was approximately linear for low applied stresses with a distinct transition to a non-linear material behavior at axial strains greater than 1Ð2% [55]. The saturated density of the soil is about 1,600 kg/cu.m [55], and the bulk density at soil water contents of 20Ð30% is around 1,200 kg/cu.m [54]. The Van Genuchten [28, 67] parameters for the CB1 soil are discussed in the next section.

Hydro-mechanical model

A challenging aspect of the numerical simulation of a hillslope-scale problem is determining the extent of the spatial and temporal discretizations, and what initial and boundary conditions to impose on the problem. Ebel et al. [22] conducted full 3D ßuid ßow simulations based on Richards equation of variably saturated ßow in the subsurface [50] using a comprehensive FE code InHM (Integrated Hydrology Model) [68]. They simulated ßow over a portion of the sediment and fractured bedrock delineated by vertical boundaries on which they believed they could reasonably impose a no-ßow boundary condition. The spatial extent of their domain description is shown in Fig. 3.

For our purposes, the deformation in the bedrock would be too small to be of concern in the coupled solid deformation/ßuid-ßow analysis, and thus we only represent the sediment domain in our simulations. However, there are two important factors that make the present simulations signiÞcantly more demanding than the ßuid-ßow simulations conducted by Ebel et al. [22]: (a) each node in the FE mesh is now composed of 3 degrees of freedom (DOFs) in 2D (two displacement and one pressure), and 4 DOFs in 3D (three displacement and one pressure); thus, the number of equations increases very fast; and (b) the water retention curve typically exhibits a steep slope near the wetting front, necessitating a high-resolution mesh everywhere in the unsaturated zone (since the wetting front propagates through the unsaturated zone).

Considering the difÞculty with modeling the exact CB1 conditions due to the uncertainties in deÞning what constitutes a ÔsufÞcientÕ 3D representation of CB1 and what boundary conditions to impose on this model, we believe that it would be more enlightening to consider a much simpler 2D plane strain representation for now, where the boundary conditions can be constrained more easily. To this end, we selected a cross-section passing through the steepest portion of the CB1 catchment, shown as section A-A in Fig. 3, and constructed the FE mesh shown in Fig. 4. This 2D representation of the slope at CB1 is conservative in the sense that out-of-plane strengths from 3D effect emanating from lateral root cohesion, friction, etc. has been ignored. The mesh shown in Fig. 4 has 20,000 nodes and 18,981 (stabilized) quadrilateral mixed Þnite elements, resulting in a total of 60,000 DOFs.

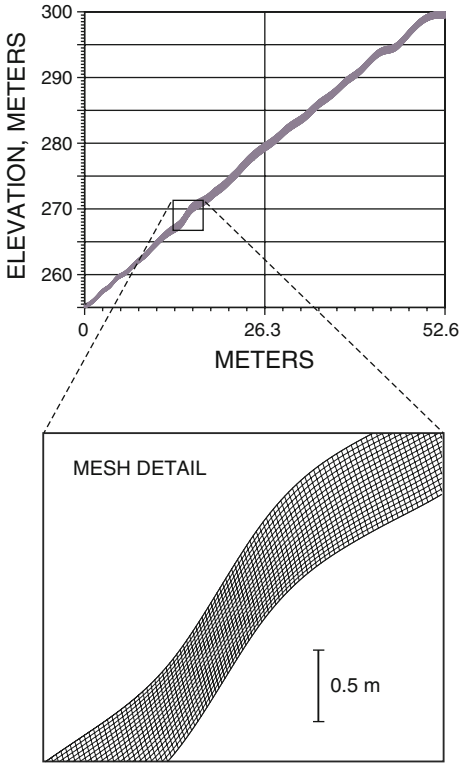

Fig. 4 Finite element mesh for CB1-like problem simulations (cf. section A-A in Fig. 3)

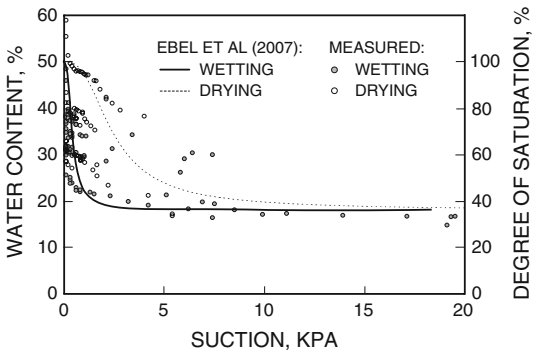

Fig. 5 Soil-water retention curve data [64] and van Genuchten curves used by Ebel et al. [22] for hydrologic simulations. We use (approximately) the Ebel et al. [22] wetting curve for the saturation-suction relation to capture the mechanical response during the wetting phase of the numerical simulations

Figures 5 and 6 show the suction/saturation and saturation/relative permeability relationships used in the simulations. The degree of saturation S_r is determined from the Van Genuchten [67] model as

$$\psi^w(s) = \psi_1 + (\psi_2 - \psi_1)\left[1 + \left(\frac{s}{s_a}\right)^n\right]^{-m}. \qquad (8)$$

The model contains four parameters: ψ_1 is the residual water saturation, ψ_2 is the maximum water saturation, n is

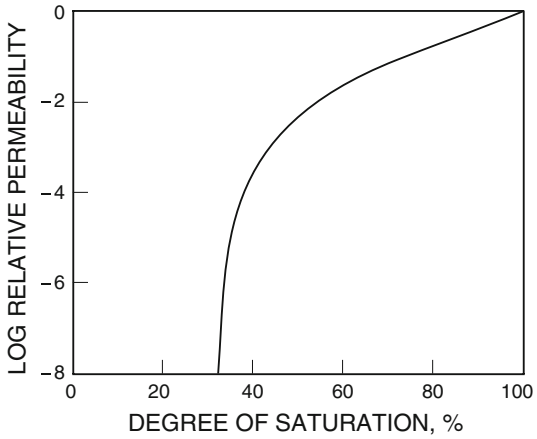

Fig. 6 Variation of relative permeability with degree of saturation based on the wetting curve

a scaling pressure, and n and m are empirical constants defining the shape of the saturation curve. The constants n and m are not independent but are rather related to one another as

$$m = \frac{n-1}{n}. \qquad (9)$$

The water phase relative permeability is similarly defined as

$$k_{rw}(\theta) = \theta^{1/2}\left[1 - \left(1 - \theta^{1/m}\right)^m\right]^2, \qquad \theta = \frac{\psi^w - \psi_1}{\psi_2 - \psi_1} \qquad (10)$$

The parameter values used in this work are given in Table 1. In order to calibrate the model, we have used the in situ retention curves as measured by Torres et al. [64] for the CB1 site. We ignored hysteretic effects and have only used the wetting measurements for calibration. The chosen values

Table 1 Material parameters

Intrinsic permeability	k	3.4×10^{-11} m^2
Fluid viscosity	μ	1.0×10^{-6} kPa s
Residual saturation	ψ_1	0.32
Maximum saturation	ψ_2	1.00
Shape constant	n	3.00
Scaling pressure	s_a	0.40 kPa
Bulk modulus	K	50 MPa
Poisson ratio	ν	0.25
Cohesion	c	0–10 kPa
Friction angle	ϕ	33–40
Dilatancy angle	ψ	$\approx 25°$
Porosity	ϕ^s	0.50
Fluid density	ρ_w	1.0 Mg/m^3
Solid density	ρ_s	2.2 Mg/m^3

are nearly the same as those used by Ebel et al. [22] in their hydrologic model except for a slight adjustment in the scaling pressure. The steep geometry of the saturation and relative permeability relationships proved to be numerically challenging on the relatively coarse mesh, and a slight flattening of the curve improved the robustness of the model.

The elastic parameters E and ν are typical for sand/gravel mixture subjected to a confining pressure comparable to those prevailing in the CB1 sediment [36]. The elastic parameters influence the displacements of the sediment but have little effect on the mechanism of failure, which is determined largely by the plasticity model. The parameters of the Mohr–Coulomb plasticity model are the cohesion c, friction angle ϕ, and dilatancy angle ψ, and their range of values is also summarized in Table 1.

5 Results

In general, failure mechanisms generated by the 2D slope model are complex and very much dependent on the imposed flow boundary conditions. Furthermore, the timing and location of initial failure are dependent on the intensity of rainfall and local flow conditions, such as the presence of a source or sink. In this section, we summarize the results of numerical simulations on the 2D slope model. The section is divided into two parts. In the first part, we show the impact of flow boundary conditions on the resulting deformation and failure patterns. In the second part, we conduct parametric studies to investigate the sensitivity of the calculated deformation and failure patterns to variation in material parameters.

5.1 Impact of flow boundary conditions

We consider three fluid-flow boundary conditions—Case A: a zero fluid pressure is prescribed on the slope surface; Case B: rainfall infiltration is prescribed on the slope surface in the form of fluid flux; and Case C: fluid infiltration into the sediment is prescribed on the interface between the sediment and fractured bedrock. The materials parameters are summarized in Table 1. For the present simulations, baseline

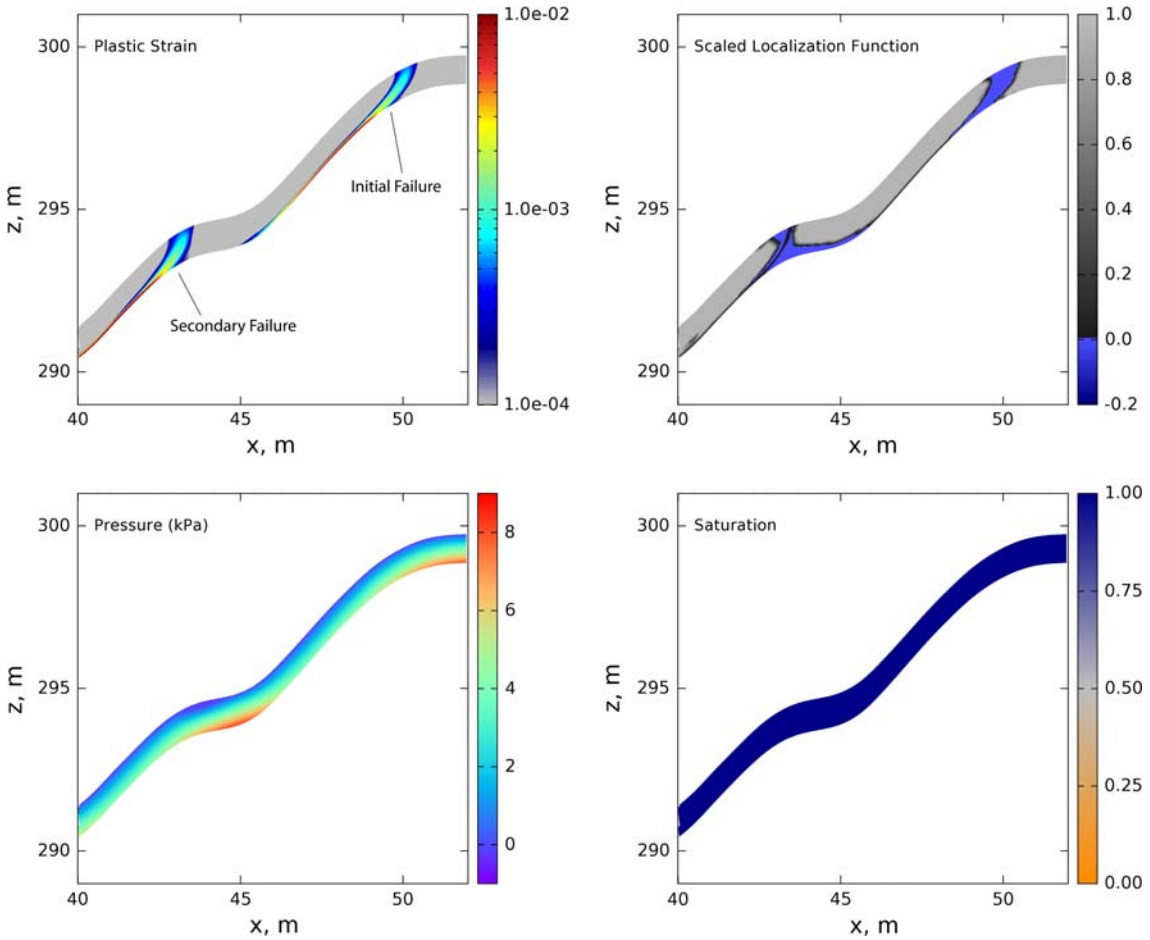

Fig. 7 Multiple slide block mechanism in a steep hillside slope subjected to rising pore water pressure boundary condition from −1.5 kPa up to 0 kPa in 3 h on slope surface

values of $c = 4$ kPa for cohesion, $\phi = 40°$ for friction angle, and $\psi = 25°$ for dilatancy angle were used.

In all the simulations, the sediment was assumed fixed to the bedrock, and any relative sliding between the sediment and bedrock may only take place in the form of plastic deformation on the sediment. The slope is very thin compared to its length, so the displacement boundary conditions on the top and bottom ends of the slope are expected to play very minor role on the calculated mechanical responses. Thus, in the present simulations, we simply assumed the top and bottom ends of the slope to be fixed to the support. However, initial conditions do play a significant role on the hydro-mechanical responses, particularly the initial value of negative pore water pressure within the sediment. Based on the hydrologic simulations of Ebel et al. [22], we assumed an initial pore water pressure of −1.5 kPa throughout the sediment. Gravity load was turned on along with this initial pore water pressure to obtain the initial effective stresses, after which the nodal displacements were reset to zero. A standard 2×2 Gauss integration rule was used for the stabilized quadrilateral mixed elements, and a backward implicit scheme was used for time integration.

For Case A, we assumed the pore water pressure on the slope surface to ramp up linearly from −1.5 kPa at $t = 0$, to 0 kPa at $t = 3$ h (Dirichlet boundary condition), with all other fluid-flow boundaries assumed to be impermeable (Neumann boundary condition). This represents a heavy rainfall, enough to saturate the slope surface within a period of 3 h and keep it saturated thereafter. Figure 7 summarizes the calculated hydro-mechanical responses at the inception of primary and secondary failure mechanisms within the slope. The general mechanism is as follows. As the sediment becomes saturated, local plastic zones develop on the base and stretch the slope segments unevenly. Eventually, plastic zones curve upwards due to local stretching of the slope segments and emerge on the ground surface approximately at coordinates $x = 43$ and 50 m. The resulting slope failure mechanism is similar to multiple slide block described by Varnes [59]. Drained bifurcation analyses based on the Rudnicki and Rice [51] procedure allowed the calculation of localization function [4, 5, 11, 12, 13, 14, 52], showing negative values. This suggests that a shear band-type bifurcation is likely to occur where the plastic deformation concentrates. On a related note, Borja [10] demonstrated that

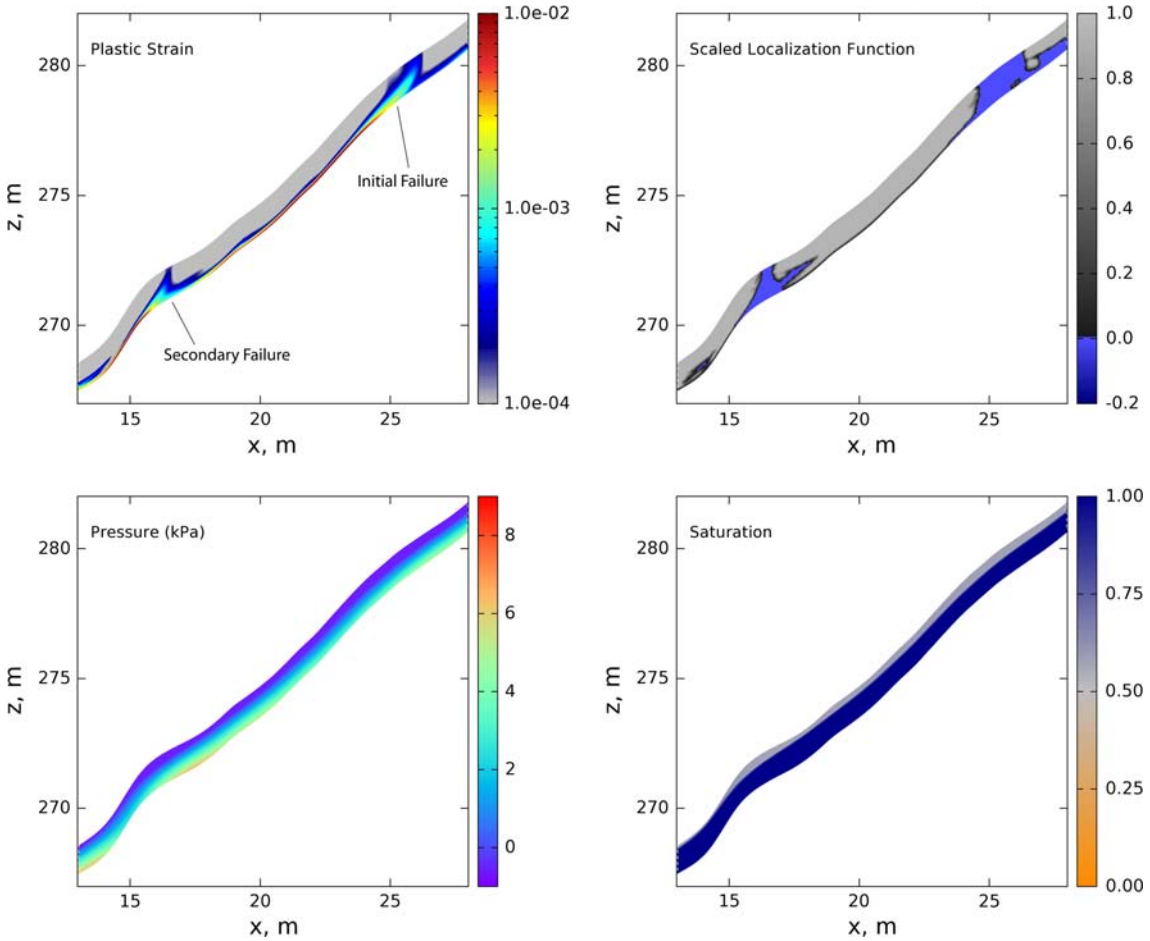

Fig. 8 Multiple slide block mechanism in a steep hillside slope subjected to rainfall infiltration of 15 mm/h on slope surface

drained shear-band bifurcation is likely to be more critical than undrained bifurcation in partially saturated dilatant frictional materials. At the inception of initial and secondary failure mechanisms, the critical slope segment is nearly saturated, and the pore water pressure is approximately hydrostatic relative to the slope surface.

For Case B, we specified a seepage infiltration of 15 mm/h on the slope surface (Neumann boundary condition) while maintaining the same flow boundary conditions on the other faces as in Case A (an initial all-Neumann set of flow boundary conditions). This eventually caused the bottom end of the slope to become saturated and the pore water pressure there to rise indefinitely. Since the pore water pressure cannot exceed zero on the slope surface, the boundary condition switched from a seepage type (Neumann) to a pressure-type (Dirichlet) on the slope surface where the pore water pressure reached zero. Figure 8 shows the calculated hydro-mechanical responses. The failure mechanism is similar to a multiple block type as in Case A, but note that the new boundary conditions have mobilized failure within a different segment of the slope (at $x = 16$ and 25 m). The localization function also shows a propensity of the sediment to develop shear strain localization where plastic deformation concentrates. Furthermore, even though the sediment is saturated all throughout the depth near the bottom end of the slope, initial failure still developed upslope, at $x = 25$ m where the sediment is still partially saturated. This suggests that the sediment does not have to be completely saturated to experience failure by plastic deformation and shear strain localization.

For Case C, we also assumed an initial all-Neumann boundary condition with zero flux on all surface boundaries except over a finite segment between $x = 12$ and 18 m on the sediment–bedrock interface. Thus, this segment of the fractured bedrock was assumed to be a fluid source. There has been much speculation about the fluid flux from the fractured bedrock at CB1. Whereas its importance on the hydrologic aspects has been elucidated from previous fluid-flow simulations [22], its impact on the sediment mechanical responses is poorly understood. To isolate the effect of fluid infiltration from the fractured bedrock, we assumed the top surface to be a no-flux boundary unless the pressure plume

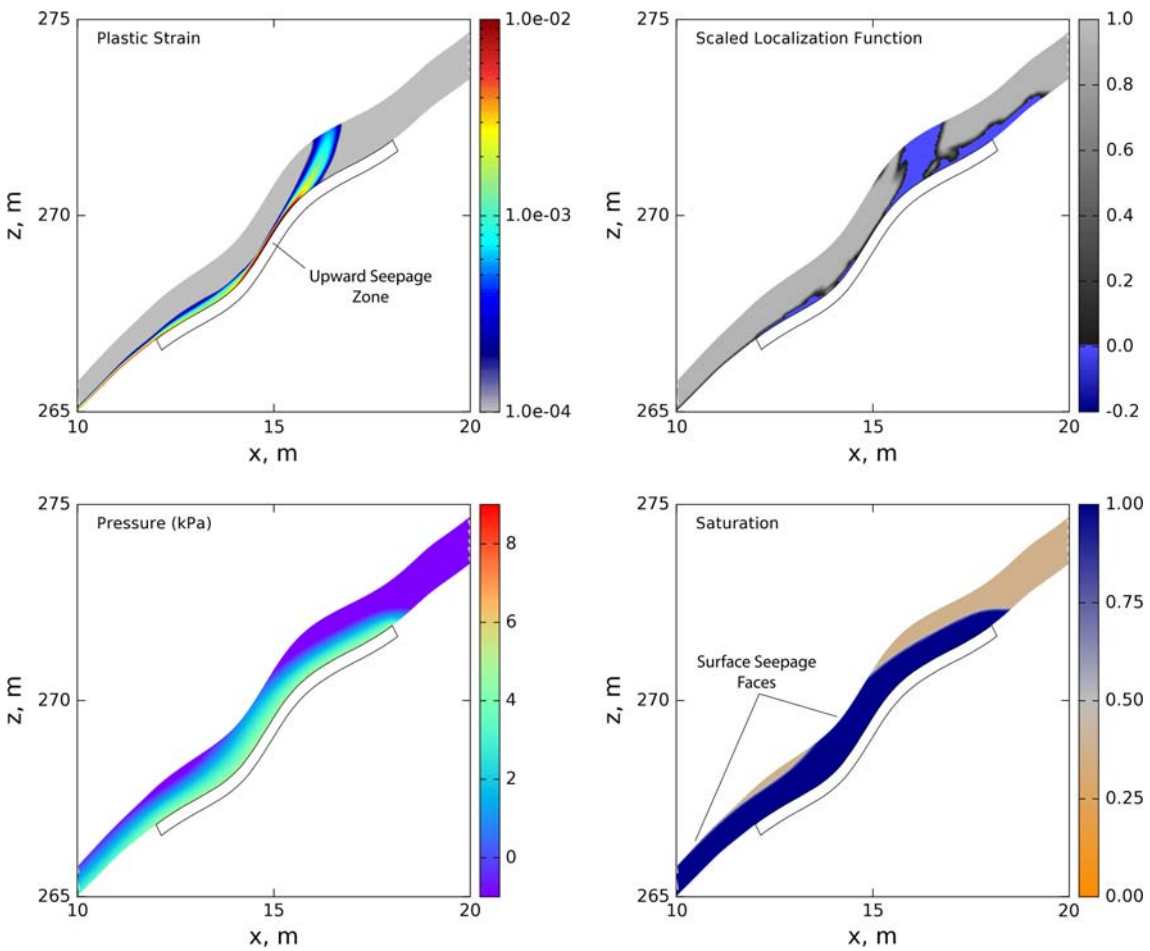

Fig. 9 Failure mechanism in a steep hillside slope subjected to upward seepage on the base of the slope

reaches it, at which point it switches to a $p_a = 0$ face. Figure 9 suggests that with only fluid influx from the fractured bedrock, it takes a large amount of seepage to build up enough pressure to fail the slope. Note that the pressure plume extends all the way to the surface, implying that upward seepage would be observed at the surface. It thus appears that upward seepage is unlikely to be the primary failure mechanism for a slope similar to CB1. However, upward seepage could certainly aggravate a slope that has already been weakened by other infiltration.

5.2 Impact of strength parameters variation on failure mechanism

The comprehensive hydrologic FE simulations conducted by Ebel et al. [22] highlighted the importance of being able

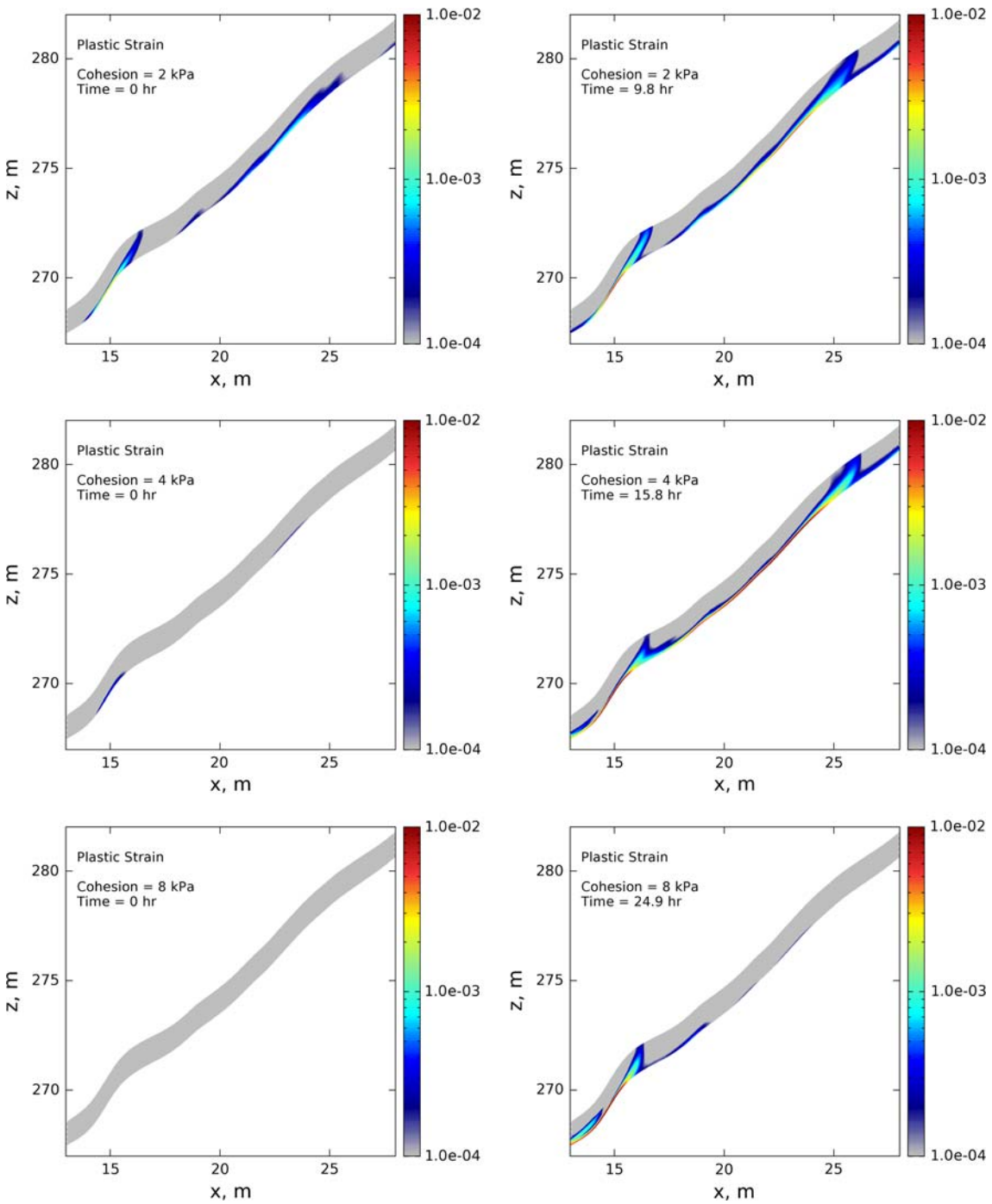

Fig. 10 Variation of failure mechanism and timing of failure with cohesion

to constrain the parameters of the ßuid-ßow model in gen eral, and the soil-water retention curve in particular, for a realistic prediction of the Þeld responses at CB1. In this section, we address the implications of uncertain strengt parameters on the predicted failure mechanism and th timing of such mechanism for a steep hillside slope similar to CB1. Fortunately, the perfectly plastic MohrÐCoulomb model has only three strength parameters: cohesion, friction angle ϕ, and dilatancy angle ψ, and thus the parametric studies can be conducted with relative ease. Any unknow hardening or softening responses may be viewed as part the uncertainties in these strength parameters.

Figure 10 shows the impact of an uncertain cohesion on the failure mechanism for the 2D slope model. The friction and dilatancy angles were Þxed at 40 and 25°, respectively, and the loading condition was deÞned by Case B (prescribe seepage on the slope face). We recall that at the CB1 site, t parameter c was derived mainly from lateral root cohesion, which could vary in space and time. For example, as the sediment is stretched, the root strength could be mobilized resulting in an increase in c, but it could also subsequently decrease when the roots are pulled from the host sedimer The Þgure shows the failure mechanisms and timing o failure at cohesion of 2, 4, and 8 kPa. At 2 kPa the slope failed for the initial conÞguration, just under its own self-weight. The observed trends are what one would expec larger cohesion delays the timing of failure. However, at $c = 8$ kPa, only a single plastic zone emerged on the slop face, not multiple ones.

Figure 11 shows the impact of an uncertain friction angle ϕ on the failure mechanism for the 2D slope model. In the simulations c was Þxed at 4 kPa, and the loading condition was again deÞned by Case B. For the two values of friction angle tested ($\phi = 30$ and 40°), the initial plastic zone emerged on the slope face at approximately the same location (at $x = 25$ m). However, for $\phi = 30°$, the secondary failure zone developed at an earlier time and above the initial failure zone (at $x = 30$ m), whereas for $\phi = 40°$, the secondary plastic zone emerged on the slope face at a later time and below the initial failure zone (at $x = 17$ m).

Finally, we consider the effect of the dilatancy angle on the predicted failure kinematics. Figure 12 compares the plastic strain distribution in the slope using two dilatancy angles, 10 and 25°, while the friction angle remains Þxed at the baseline value of 40°. In both cases, a failure surface extending to slope surface is observed at approximately $x = 25$ m, suggesting that this failure mode is insensitive to dilatancy. In the low dilatancy angle simulation, however, the secondary failure in the $x = 16$ m region is suppressed. There is some indication that with additional deformation, a secondary failure may initiate at this point, but the timing of the two would not be as closely linked as in the high dilatancy angle case. Close examination of the plastic strain contours in both simulations

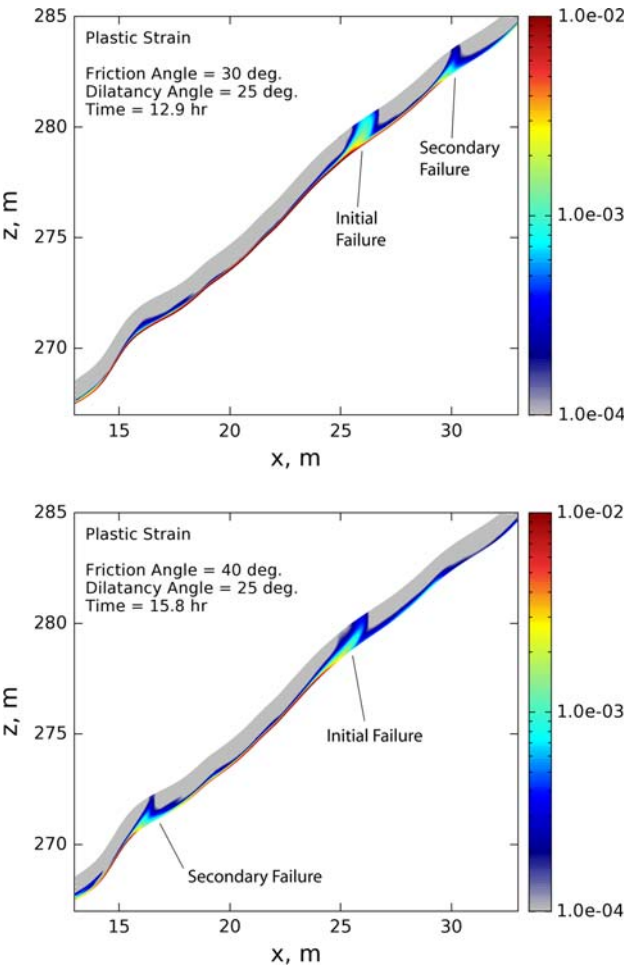

Fig. 11 Variation of failure mechanism and timing of failure with friction angle

also indicate that the plastic zone in the low dilatancy case is less ÔÔdiffuseÕÕ than in the high dilatancy case.

We remark that many interesting features of the coupled physics in this problem are spatially localized. For example, consider the sharp wetting front that moves through the domain, or the localized plastic shear deformation. From a computational perspective, this suggests that an adaptive mesh reÞnement algorithm could be quite useful for this class of problems. This assessment is particularly true as one considers fully three-dimensional analyses in complex domains. However, there are at least two non-trivial issues that must be addressed in order to apply this algorithm to coupled ßuid-ßow/solid-deformation problems. The Þrst is that an appropriate reÞnement/coarsening criterion must be developed that accounts for the coupled nature of the ßuid-solid problem, see [23, 56]. The second consideration is that applying adaptive mesh reÞnement to a plastic medium introduces additional questions about how to handle the treatment of internal plastic variables. When an element is reÞned or coarsened, new quadrature points are created, and the internal plastic history of the material must be

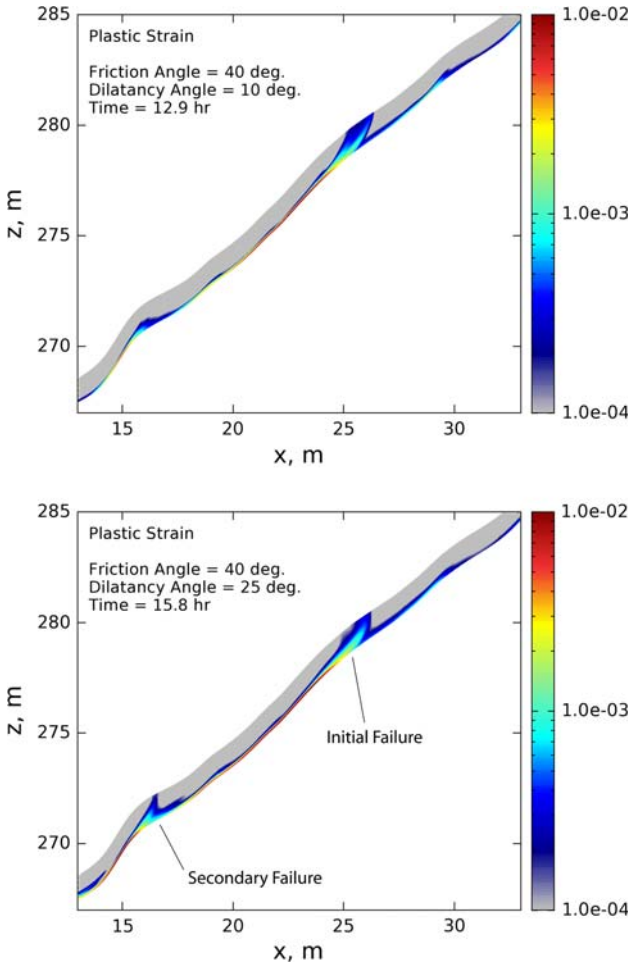

Fig. 12 Variation of failure mechanism and timing of failure with dilatancy angle

transferred to these new points. For a simple plasticity model (such as MC), a straightforward projection/interpolation method may be sufÞcient, but for more complex models (say, a critical state soil model) with several internal parameters, we must develop a reÞnement strategy that ensures that the plastic variables remain self-consistent with one another as projection or interpolation operations proceed, see [16, 38, 48].

6 Summary and conclusions

We have presented a continuum physics-based framework for analysis of coupled solid deformation-ßuid-ßow processes in partially saturated earthen slopes. The formulation for constitutive modeling of the unsaturated sediment is based on the use of an effective stress measure that represents the sole stress state variable responsible for deforming the solid skeleton, and on direct use of suction in the constitutive relations [10, 11, 15, 33]. Other alternative approaches exist, in which different pairs of stress state variables are chosen instead of a single effective stress, such as the net stress and matric suction [24, 25, 70Ð72]. However, the effective stress used in this work appears to have an advantage in terms of FE implementation, since the coupled formulation follows exactly the same lines as those developed for the fully saturated case. This implies that stabilized low-order mixed FE elements can be used just as well for the unsaturated case.

We have used the coupled continuum FE model to analyze the deformation and stability of a steep hillside slope similar to the CB1 site. Despite the simpliÞed 2D plane strain representation adopted by the model, the predicted failure mechanisms are complex and nowhere near what one would normally obtain from an inÞnite slope assumption. For a steep hillside slope similar to CB1, it appears that failure mechanism would likely initiate in the form of multiple failure blocks, which could transform into a debris ßow similar to what was observed at the CB1 site during the November 1996 event. An obvious advantage of the proposed continuum modeling approach lies in its ability to integrate important hydro-mechanical processes responsible for triggering rainfall-induced movement of earthen slopes, including increased saturation, ßuid ßow, and inelastic solid deformation. Work is currently underway to incorporate 3D effects into the numerical model.

Acknowledgments This work is supported by the US National Science Foundation under Contract Numbers CMMI-0824440 and CMMI-0936421 to Stanford University. The second author acknowledges support from the US National Science Foundation Graduate Research Fellowship and the Stanford Graduate Fellowship Programs. We wish to thank Drs. Keith Loague and Brian Ebel for numerous discussions pertaining to the CB1 problem. We are also grateful to two anonymous reviewers for their constructive reviews.

References

1. Alonso EE, Gens A, Josa A (1990) A constitutive model for partially saturated soils. Geotechnique 40:405Ð430
2. Anderson SP (1995) Flow paths, solute sources, weathering, and denudation rates: the chemical geomorphology of a small catchment. PhD Dissertation, University of California, Berkeley
3. Anderson SP, Dietrich WE, Montgomery DR, Torres R, Conrad ME, Loague K (1997) Subsurface ßowpaths in a steep, unchanneled catchment. Water Resour Res 33:2637Ð2653
4. Andrade JE, Borja RI (2006) Capturing strain localization in dense sands with random density. Int J Numer Methods Eng 67:1531Ð1564
5. Andrade JE, Borja RI (2007) Modeling deformation banding in dense and loose ßuid-saturated sands. Finite Elem Anal Design 43:361Ð383
6. AriÞn YF, Schanz T (2009) Osmotic suction of highly plastic clays. Acta Geotech 4:177Ð191
7. Birle E, Heyer D, Vogt N (2008) Inßuence of the initial water content and dry density on the soil-water retention curve and the shrinkage behavior of a compacted clay. Acta Geotech 3:191Ð200

8. Bochev PB, Dohrmann CR, Gunzburger MD (2006) Stabilization of low-order mixed Þnite elements for the Stokes equations. SIAM J Numer Anal 44:82Ð101
9. Bochev PB, Dohrmann CR (2006) A computational study of stabilized, low-order C^0 Þnite element approximations of Darcy equations. Comput Mech 38:323Ð333
10. Borja RI (2004) Cam-Clay plasticity, part V: a mathematical framework for three-phase deformation and strain localization analyses of partially saturated porous media. Comput Methods Appl Mech Eng 193:5301Ð5338
11. Borja RI (2006) On the mechanical energy and effective stress in saturated and unsaturated porous continua. Int J Solids Struct 43:1764Ð1786
12. Borja RI, Andrade JE (2006) Critical state plasticity. Part VI: Meso-scale Þnite element simulation of strain localization in discrete granular materials. Comput Methods Appl Mech Eng 195:5115Ð5140
13. Borja RI (2006) Conditions for instabilities in collapsible solids including volume implosion and compaction banding. Acta Geotech 1:107Ð122
14. Borja RI (2006) Condition for liquefaction instability in ßuid-saturated granular soils. Acta Geotech 1:211Ð224
15. Borja RI, Koliji A (2009) On the effective stress in unsaturated porous continua with double porosity. J Mech Phys Solids 57:1182Ð1193
16. Boroomand B, Zienkiewicz OC (1999) Recovery procedures in error estimation and adaptivity. Part II: adaptivity in nonlinear problems of elasto-plasticity behaviour. Comput Methods Appl Mech Eng 176:127Ð146
17. Brooks SM, Crozier MJ, Preston NJ, Anderson MG (2002) Regolith stripping and the control of shallow translational hill-slope failure: application of a two-dimensional coupled soil hydrology-slope stability model, HawkeÕs Bay, New Zealand. Geomorphology 45:165Ð179
18. Brown WM III, Sitar N, Saarinen TF, Blair ML (1984) Debris ßows, landslides, and ßoods in the San Francisco Bay region, January 1982. In: Overview of and summary of a conference held at Stanford University, August 23Ð26, 1982, Washington D.C., National Research Council and USGS, 83 pp
19. Burroughs ER Jr, Hammond CJ, Booth GD (1985) Relative stability estimation for potential debris avalanche sites using Þeld data. In: Proceedings of the international symposium on erosion, debris ßow and disaster prevention, Tsukuba, pp 335Ð339
20. Dohrmann CR, Bochev PB (2004) A stabilized Þnite element method for the Stokes problem based on polynomial pressure projections. Int J Numer Methods Fluids 46:183Ð201
21. Ebel BA, Loague K, Dietrich WE, Montgomery DR, Torres R, Anderson SP, Giambelluca TW (2007) Near-surface hydrologic response for a steep, unchanneled catchment near Coos Bay, Oregon: 1. Sprinkling experiments. Am J Sci 307:678Ð708
22. Ebel BA, Loague K, VanderKwaak JE, Dietrich WE, Montgomery DR, Torres R, Anderson SP (2007) Near-surface hydrologic response for a steep, unchanneled catchment near Coos Bay, Oregon: 2. Physics-based simulations. Am J Sci 307:709Ð748
23. Ehlers W, Ammann M, Diebels S (2002) h-Adaptive FE methods applied to single-and multiphase problems. Int J Numer Meth Eng 54:219Ð239
24. Fredlund DG, Morgenstern NR (1977) Stress state variables for unsaturated soils. J Geotech Eng Div ASCE 103:354Ð358
25. Gallipoli G, Gens A, Sharma R, Vaunat J (2003) An elasto-plastic model for unsaturated soil incorporating the effects of suction and degree of saturation on mechanical behaviour. Geotechnique 53:123Ð135
26. Houlsby GT (1979) The work input to a granular material. Geotechnique 29:354Ð358
27. Houlsby GT (1997) The work input to an unsaturated granular material. Geotechnique 47:193Ð196
28. Houston SL, Houston WN, Zapata C, Manepally C, Lawrence C (1999) Inßuence of compressibility on use and interpretation of soil water characteristic curve. In: Proceedings of the XI Pan-American conference on soil mechanics and geotechnical engineering, Foz do Iguassu, pp 947Ð954
29. Iverson RM (2000) Landslide triggering by rain inÞltration. Water Resour Res 36:1897Ð1910
30. Jha B, Juanes R (2007) A locally conservative Þnite element framework for the simulation of coupled ßow and reservoir geomechanics. Acta Geotech 2:132Ð153
31. Jibson RW (1992) The Mameyes, Puerto Rico, landslide disaster of October, 7, 1985. In: Slosson JE, Keene AG, Johnson JA (eds) Landslides/landslide mitigation. Reviews in Engineering Geology. Geological Society of America, Boulder, pp 37Ð54
32. Kaitna R, Rickenmann D, Schatzmann M (2007) Experimental study on rheologic behaviour of debris ßow material. Acta Geotech 2:71Ð85
33. Koliji A, Vulliet L, Laloui L (2008) New basis for the constitutive modelling of aggregated soils. Acta Geotech 3:61Ð69
34. Khalili N, Geiser F, Blight GE (2004) Effective stress in unsaturated soils: review with new evidence. Int J Geomech 4:115Ð126
35. Kim J, Jeong S, Park S, Sharma J (2004) Inßuence of rainfall-induced wetting on the stability of slopes in weathered soils. Eng Geol 75:251Ð262
36. Lambe TW, Whitman RV (1969) Soil mechanics. Wiley, New York
37. Lagmay AMA, Ong JBT, Fernandez DFD, Lapus MR, Rodolfo RS, Tengonciang AMP, Soria JLA, Baliatan EG, Quimba ZL, Uichanco CL, Paguican EMR, Remedio ARC, Lorenzo GRH, Avila FB, Valdivia W (2006). Scientists investigate recent Philippine landslide. Eos Trans AGU 87(12):121
38. Lee NS, Bathe KJ (1994) Error indicators and adaptive remeshing in large deformation Þnite element analysis. Finite Elem Anal Design 16:99Ð139
39. Lu N, Likos WJ (2006) Suction stress characteristic curve for unsaturated soil. J Geotech Eng 132:131Ð142
40. Lu N, Likos WJ (2004) Unsaturated soil mechanics. Wiley, Hoboken
41. MartÕnez E (2002) Evento Meteorológico sobre el Litoral Central en Diciembre 1999. Informe inédito
42. Montgomery DR (1991) Channel initiation and landscape evolution. PhD Dissertation, University of California, Berkeley
43. Montgomery DR, Dietrich WE, Torres R, Anderson SP, Heffner JT, Loague K (1997) Hydrologic response of a steep, unchanneled valley to natural and applied rainfall. Water Resour Res 33:91Ð109
44. Moriguchi S, Borja RI, Yashima A, Sawada K (2009) Estimating the impact force generated by granular ßow on a rigid obstruction. Acta Geotech 4:57Ð71
45. Nur A, Byerlee JD (1971) An exact effective stress law for elastic deformation of rock with ßuids. J Geophys Res 76:6414Ð6419
46. Nuth M, Laloui L (2008) Effective stress concept in unsaturated soils: clariÞcation and validation of a uniÞed framework. Int J Numer Anal Methods Geomech 32:771Ð801
47. Okura Y, Kitahara H, Ochiai H, Sammori T, Kawanami A (2002) Landslide ßuidization process by ßume experiments. Eng Geol 66:65Ð78
48. Peric D, Hochard C, Dutko M, Owen DRJ (1996) Transfer operators for evolving meshes in small strain elasto-placticity. Comput Methods Appl Mech Eng 137:331Ð344
49. Rahardjo H, Li XW, Toll DG, Leong EC (2001) The effect of antecedent rainfall on slope stability. Geotech Geol Eng 19:371Ð399

50. Richards LA (1931) Capillary conduction of liquids in porous mediums. Physics 1:318Ð333
51. Rudnicki JW, Rice JR (1975) Conditions for the localization of deformation in pressure-sensitive dilatant materials. J Mech Phys Solids 23:371Ð394
52. Runesson K, Ottosen NS, Peric D (1991) Discontinuous bifurcations of elastic-plastic solutions at plane stress and plane strain. Int J Plast 7:99Ð121
53. Schmidt KM (1994) Mountain scale strength properties, deep-seated landsliding and relief limits. MS Thesis, Department of Geological Sciences, University of Washington, Seattle
54. Schmidt KM (1999) Root strength, colluvial soil depth, and colluvial transport on landslide-prone hillslopes. PhD Dissertation, Department of Geological Sciences, University of Washington, Seattle
55. Schmidt KM, Roering JJ, Stock JD, Dietrich WE, Montgomery DR, Schaub T (2001) The variability of root cohesion as an inßuence on shallow landslide susceptibility in the Oregon Coast Range. Can Geotech J 38:995Ð1024
56. Schreßer BA, Secchi S, Simoni L (2006) On adaptive reÞnement techniques in multi-Þeld problems including cohesive fracture. Comput Methods Appl Mech Eng 195:444Ð461
57. Schroeder WL, Alto JV (1983) Soil properties for slope stability analysis; Oregon and Washington coastal mountains. For Sci 29:823Ð833
58. Schuster RL, Salcedo DA, Valenzuela L (2002) Overview of catastrophic landslides of South America in the twentieth century. In: Evans SG, DeGraff JV (eds) Catastrophic landslides effects, occurrence, and mechanisms. Reviews in Engineering Geology, Geological Society of America, Boulder, pp 1Ð33
59. Sidle, RC (1992) A theoretical model of the effects of timber harvesting on slope stability. Water Resour Res 28:1897Ð1910
60. Skempton AW (1961) Effective stress in soils, concrete and rocks. In: Pore pressure and suction in soils, Butterworths, London, pp 4Ð16
61. Smith TC, Hart EW (1982) Landslides and related storm damage, January 1982, San Francisco Bay region. Calif Geol 35:139Ð152
62. Terzaghi K (1943) Theoretical soil mechanics. Wiley, New York
63. Torres R (1997) Unsaturated zone processes and the hydrologic response of a steep, unchanneled valley. PhD Dissertation, University of California, Berkeley
64. Torres R, Dietrich WE, Montgomery DR, Anderson SP, Loague K (1998) Unsaturated zone processes and the hydrologic response of a steep, unchanneled catchment. Water Resour Res 34:1865Ð1879
65. USAID (2000) Venezuela factsheet, February, 2000. USAID-OfÞce of Foreign Disaster Assistance, 2 pp
66. Van Sint Jan M, Talloni P (1993) Flujo de sedimentos del 18 de Juniode 1991 en Antofagosta: La Serena, Chile. Tercer Congreso Chileno de Ingenieria Geotecnia 1:247Ð265
67. Van Genuchten MT (1980) A closed-form equation for predicting the hydraulic conductivity of unsaturated soils. Soil Sci Soc Am J 44:892Ð898
68. VanderKwaak JE (1999) Numerical simulation of ßow and chemical transport in integrated surface-subsurface hydrologic systems. PhD Dissertation, University of Waterloo, Waterloo
69. Varnes DJ (1978) Slope movement types and processes. In: Schuster RL, Krizek RJ (eds) Landslides analysis and control. Special Report 176, National Academy of Sciences, Washington
70. Vaunat J, Cante JC, Ledesma A, Gens A (2000) A stress point algorithm for an elastoplastic model in unsaturated soils, Int J Plast 16:121Ð141
71. Wheeler SJ, Sivakumar V (1995) An elasto-plastic critical state framework for unsaturated soil. Geotechnique 45:35Ð53
72. Wheeler SJ, Gallipoli D, Karstunen M (2002) Comments on the use of Barcelona Basic Model for unsaturated soils. Int J Numer Anal Methods Geomech 26:1561Ð1571
73. White JA, Borja RI (2008) Stabilized low-order Þnite elements for coupled solid-deformation/ßuid-diffusion and their application to fault zone transients. Comput Methods Appl Mech Eng 197:4353Ð4366
74. Wu TH, Beal PE, Lan C (1988) In-situ shear test of soil-root systems. J Geotech Eng ASCE 114:1376Ð1394
75. Yee CS, Harr DR (1977) Inßuence of soil aggregation on slope stability in the Oregon Coast Range. Environ Geol 1:367Ð377
76. Young YL, White JA, Xiao H, Borja RI (2009) Liquefaction potential of coastal slopes induced by solitary waves. Acta Geotech 4:17Ð34